The Athena X-ray Integral Field Unit (X-IFU)

F. Pajot[1], **D. Barret**[1], **T. Lam-Trong**[2], **J-W. den Herder**[3], **L. Piro**[4], **M. Cappi**[5], **J. Huovelin**[6], **R. Kelley**[7], **J. M. Mas-Hesse**[8], **K. Mitsuda**[9], **S. Paltani**[10], **G. Rauw**[11], **A. Rozanska**[12], **J. Wilms**[13], **M. Barbera**[14], **F. Douchin**[2], **H. Geoffray**[2], **R. den Hartog**[3], **C. Kilbourne**[7], **M. Le Du**[2], **C. Macculi**[4], **J-M. Mesnager**[2], **P. Peille**[2]

the date of receipt and acceptance should be inserted later

Abstract The X-ray Integral Field Unit (X-IFU) of the Advanced Telescope for High-ENergy Astrophysics (Athena) large-scale mission of ESA will provide spatially resolved high-resolution X-ray spectroscopy from 0.2 to 12 keV, with 5" pixels over a field of view of 5 arc minute equivalent diameter and a spectral resolution of 2.5 eV (FWHM) up to 7 keV. The core scientific objectives of Athena drive the main performance parameters of the X-IFU. We present the current reference configuration of the X-IFU, and the key issues driving the design of the instrument.

Keywords X-ray astronomy, imaging spectroscopy, microcalorimeter

Contact: François Pajot
E-mail: francois.pajot@irap.omp.eu

[1] IRAP CNRS/Université Paul Sabatier, 9 av. du colonel Roche, 31028 Toulouse cedex 4, France
[2] CNES, 18 av. Edouard Belin, 31401 Toulouse cedex 9, France
[3] SRON, Sorbonnelaan 2, 3584 CA Utrecht, The Netherlands
[4] INAF/IAPS, via Fosso del Cavaliere 100, 00133 Roma, Italy
[5] INAF-IASF, via Gobetti 101, 40129 Bologna, Italy
[6] Department of Physics, Division of Geophysics and Astronomy, P.O. Box 48, FI-00014, University of Helsinki, Finland
[7] NASA/Goddard Space Flight Center, 8800 Greenbelt Rd, Greenbelt, MD 20771, United States
[8] Centro de Astrobiología, CSIC / INTA, Ctra de Torrejón a Ajalvir, 4 km, 28850 Torrejón de Ardoz, Madrid, Spain
[9] Institute of Space and Astronautical Science (ISAS) & Japan Aerospace Exploration Agency (JAXA), 3-1-1 Yoshinodai, Chuo-ku, Sagamihara, 252-5210, Japan
[10] Department of Astronomy, University of Geneva, Chemin d'Ecogia 16, CH-1290 Versoix, Switzerland
[11] University of Liège, Institute for Astrophysics & Geophysics, Allée du 6 Août 19c, B-4000 Liège, Belgium
[12] Nicolaus Copernicus Astronomical Centre of the Polish Academy of Sciences, ul. Bartycka 18, 00-716 Warsaw, Poland
[13] ECAP, University of Erlangen-Nüremberg, Sternwartstr. 7, 96049 Bamberg, Germany
[14] Università degli Studi di Palermo, Dipartimento di Fisica e Chimica, Via Archira 36, 90123 Palermo, Italy & INAF/Osservatorio Astronomico di Palermo G.S.Vaiana, Piazza del Parlamento 1, 90134 Palermo, Italy

1 Athena and the X-ray Integral Field Unit

Athena is the second large mission (L2) of the European Space Agency Cosmic Vision program, dedicated to the study of the hot and energetic Universe. The mission is presently undergoing a feasibility study both at spacecraft and instrument levels and its launch is planned in 2029/2030. Two focal plane instruments, the Wide Field Imager (WFI) optimized for surveys and the X-ray Integral Field Unit (X-IFU) optimized for spatially resolved high spectral resolution spectroscopy, will benefit from an unprecedented collecting area in the X-rays (1.4 m^2 at 1 keV) and an angular resolution of 5". The X-IFU will give access to integral field spectroscopy thanks to an array of 3840 transition edge sensors (TES) microcalorimeters operated with a 50 mK base temperature, with an energy resolution improved by a factor of two and a number of pixels two orders of magnitude larger than any X-ray high resolution spectral imager ever sent to space (e.g. Hitomi/SXS [1, 2]). Fig. 1 illustrates the potential gains of the Athena/X-IFU both in effective area and weak line sensitivity factor of merit with respect to present and near future missions.
The purpose of this paper is not to give a detailed description of the Athena mission and X-IFU instrument, available in [3] and [4], but to give a status of the on-going technology developments required as part of the instrument feasibility study phase. The scientific requirements of the mission relevant to the X-IFU are reported in Table 1. The status of the key subsystems driving the performance is presented in the following sections, referring as needed to the corresponding publications in this special issue. A deliberate emphasis is put on the energy resolution as a capability unique to the X-IFU.

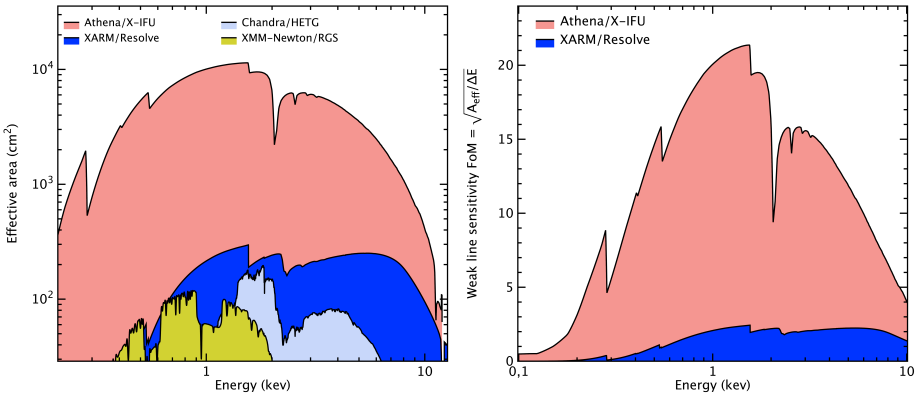

Fig. 1 (*Left*) Effective area of the Athena/X-IFU instrument compared to current (Chandra/HEGT, XMM-Newton/RGS) or near future (XARM/Resolve, assuming the same response as Hitomi/SXS [1]) X-ray imaging spectrometers in the 0.2—12 keV energy range. (*Right*) Weak line sensitivity factor of merit of the Athena/X-IFU instrument compared to the next and only high resolution imaging spectrometer XARM/Resolve. High resolution spectrometry refers to instruments achieving a less than $\sim$ 10 eV energy resolution, a capability now enabled in space by micro-calorimeter arrays.

Table 1 Athena level requirements driving the X-IFU specifications and main subsystems impacted

Parameters	Requirements	Subsystem
Energy range	0.2—12 keV	TES array, thermal filters, FW [f] blocking filters
Energy resolution: E $<$ 7 keV	2.5 eV [a,b]	TES array, FPA [g], thermal filters, readout chain
Energy resolution: E $>$ 7 keV	$E/\Delta E = 2800$ [c,b]	TES array, FPA, thermal filters, readout chain
Field of View	5'(equivalent diameter)	TES array, FPA, aperture cylinder
Effective area @ 0.3 keV	> 1500 cm^2	TES array, thermal filters
Effective area @ 1.0 keV	> 14000 cm^2	TES array, thermal filters
Effective area @ 7.0 keV	> 1600 cm^2	TES array, thermal filters
Gain calibration error (peak, 7 keV)	0.4 eV	TES array, FPA, readout chain, cryochain, MXS [h]
Count rate capability nominally bright point sources	1 mCrab ($> 80\%$ high-res. events) [d]	TES array, thermal filters, readout chain
Count rate capability brightest point sources	1 Crab ($> 30\%$ throughput) [e]	TES array, thermal filters, readout chain
Time resolution	10 μs	TES array, readout chain
Non X-ray background (2—10 keV, 80% of the time)	$< 5\ 10^{-3}$ counts/s/cm^2/keV	CryoAC [i], TES array, FPA, dewar

[a] Goal 1.5 eV, [b] High-resolution grade events
[c] Considered linear so far (arbitrarily), but will eventually depend on the readout chain optimization
[d] Goal 10 mCrab ($> 80\%$ high-resolution events), [e] Degraded resolution (~ 30 eV)
[f] Filter Wheel (FW), [g] Focal Plane Assembly (FPA)
[h] Modulated X-ray Source (MXS), [i]Anticoincidence detector (CryoAC)

2 Detectors

The TES microcalorimeter array impacts all the X-IFU requirements. The main contributor to the energy resolution budget is intrinsic to the microcalorimeters. The allocation of 2.1 eV (Root Square Sum - RSS) drives the detector design. The operation of the TES under AC biasing, inherent to the frequency domain multiplexing (FDM) choice for the baseline readout chain, raises new challenges for the detector development: the detectors optimization presently focuses on the AC loss in the TES and AC weak-link Josephson Junction effects [5-10]. Optimization of the quantum efficiency and count rate capabilities impacts directly the detector absorber and thermal design [11, 12]. The detector baseline now takes into account the adjustable focus capability of the mirror. With a defocus of 35 mm and the critically damped time constant of 286 μs of the new Large Pixel Array baseline (LPA-2) pixels [4], the high count rate capability exceeds the goal requirements of 10 mCrab (high resolution) and an even higher count rate up to 1 Crab with 10 eV resolution can be achieved in the 5-8 keV band with use of a beryllium filter (Fig. 2) [13]. In this latter regime, the influence of crosstalk is critical to the instrument performance, as studied in [14].

3 Readout chain

The readout chain is the next subsystem to appear in the requirements. With a total allocation of 1.2 eV (RSS) it is the second contributor to the energy resolution budget. The FDM readout is based on 96 channels addressing each 40 pixels modulated in the 1-5 MHz interval

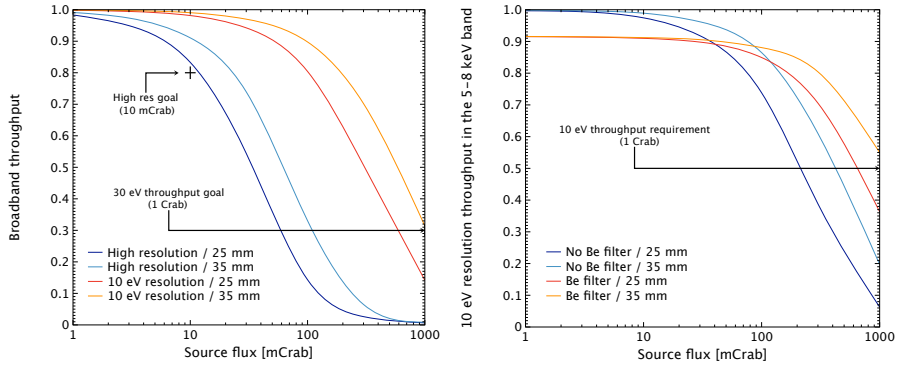

Fig. 2 (*Left*) Broadband throughput and (*Right*) 5-8 keV band throughput including use of a beryllium filter achievable with the new micro-calorimeter Large Pixel Array baseline (LPA-2) and two mirror defocusing values (25 or 35 mm)[13].

[15]. The chain includes cryogenic LC filters [16] and front-end and amplification SQUIDs located in the Focal Plane Assembly. Interconnection of the large number of pixels (3840) requires specific development [17]. The low noise amplifier based on SiGe ASIC technology is placed at room temperature in the Warm Front-End Electronics, which also drives the SQUIDs [18]. The biasing of the TES is performed in the Digital Readout Electronics (DRE), together with the Base Band Feedback (BBFB) loop that is implemented to linearize the SQUID operation. The DRE also contains an event processor based on optimal filtering and pulse templates to recover on-board the photon energy.
The Digital to Analog Converter driving the feedback signal is one of the key elements of the X-IFU chain, whose dynamic range directly impacts the instrument energy resolution. On top of its noise floor, intermodulation terms created during the generation of the carriers may create spurious signals interfering with the pixel data. An active tuning of the pixel biasing circuit resonance frequencies can be used to create a perfectly regular frequency grid to mitigate this effect as presented in [19]. The entire readout chain gain requires periodic recalibration of the overall system gain with the on-board Modulated X-ray Source (MXS) in order to correct for drifts on $\sim$ 1000 s timescale: a two parameter approach based on the pulse-height estimate of a calibration line and the baseline value of the pulses is described in [20].

4 Focal plane assembly and anticoincidence detector

The FPA is composed of the microcalorimeter array, the cryogenic stage of the readout chain (LC filters, coupling coils, front-end SQUIDs, amplifiers SQUIDs), the anticoincidence detector (CryoAC) and its cold readout. It provides shielding (thermal filters with metallic mesh on the optical path, niobium shield and mu-metal shield) in order to address radiative EMI/EMC and quasi-static magnetic field. It is a complex system whose mechanical and thermal interfaces to the 2 K stage and the sub-kelvin cooler must also comply with conductive EMI/EMC specifications.
The non-focused non X-ray background results from galactic cosmic ray interacting with

the detector array and its environment. It is rejected using the combination of information coming from microcalorimeter pixel saturation and spatial coincidence, and the active 4 TES pixels CryoAC located below it [21-24]. Unrejected background events, mostly (more than 75%) secondary electrons back scattered on the array, can be limited by an optimization of the design and material of the mechanical parts closest to the detectors: a passive shield composed of materials with low electron yield such as Kapton between the niobium shield and the detector is considered. A layer of absorber such as bismuth can further reduce the residual background by blocking secondary photons of energy in the X-IFU energy range [25].
The vetoing of non X-ray background events can thus be achieved to a very high level (in the order of 1/100 of the incoming particle flux intercepted by the detector in the 2-10 keV energy bandwidth). However a fraction of the incoming particles deposits energy in the silicon wafer supporting the detectors, similar to what was observed in Planck/HFI bolometers [26]. This results in fluctuations of the microcalorimeters bath temperature and triggered a study analog to that already carried on bolometers irradiated by high energy particles [27]. Increasing the heat sinking of the array frame or tuning its heat capacity will be implemented if need be in the detector design.

5 Aperture cylinder and cryogenic chain

Located in the optical path, the aperture cylinder holds the thermal filters that will prevent all radiation but the X-ray photons to reach the detectors. This subsystem must control the thermal radiation (IR-visible) mostly emitted by the local environment of the cryostat to ensure its cryogenic performance, reject the UV photons that would create shot noise (the filter wheel blocking filters bring additional attenuation in case of observation of bright OB stars), and attenuate the electromagnetic field coming from the satellite and the subsystems surrounding the cryostat (warm electronics, compressors) in order to control EMI [28]. In addition, the filters, standing in the path of the incoming astrophysical radiation, must stay clear of contaminant (molecular, particles) that would degrade their transmission in the X-IFU energy band.
This leads to a filter design associating very thin polyimide films on which is deposited a layer of metal, and a conductive mesh. The optimization of these meshes is required to keep the highest X-IFU quantum efficiency together with the pixel absorber design [29,30].
Hitomi and Planck are the only two space missions that have successfully and continuously operated detectors cooled at and below 100 mK. By its large number of pixels and associated cold stage electronics, the X-IFU sets a new challenge for a 50 mK cryogenic system operated in space based only on active cryocoolers. Fig. 3 presents the reference cryogenic chain based on five 15 K pulse tube coolers (PT15K), two ^{4}He Joule-Thomson 4 K coolers (4HeJT), two ^{3}He Joule-Thomson 2 K coolers (3HeJT) and one hybrid ^{3}He sorption/Adiabadic Demagnetization (ADR) sub-Kelvin cooler ensuring 50 mK base temperature for the detectors, compliant with margin and redundancy philosophy. On-going tests of a cryogenic chain including potential Joule-Thomson and sub-Kelvin space cryocoolers as a demonstration of the selected technologies are described and their performance reported in [31].
The 0.6 eV (RSS) contribution to the energy resolution budget attributed to the aperture

cylinder and the cryogenic chain comes from the 50 mK thermal stability (0.9 μK rms, 3 μK drifts between MXS recalibrations), and system level contributors such as microvibrations and EMI/EMC.

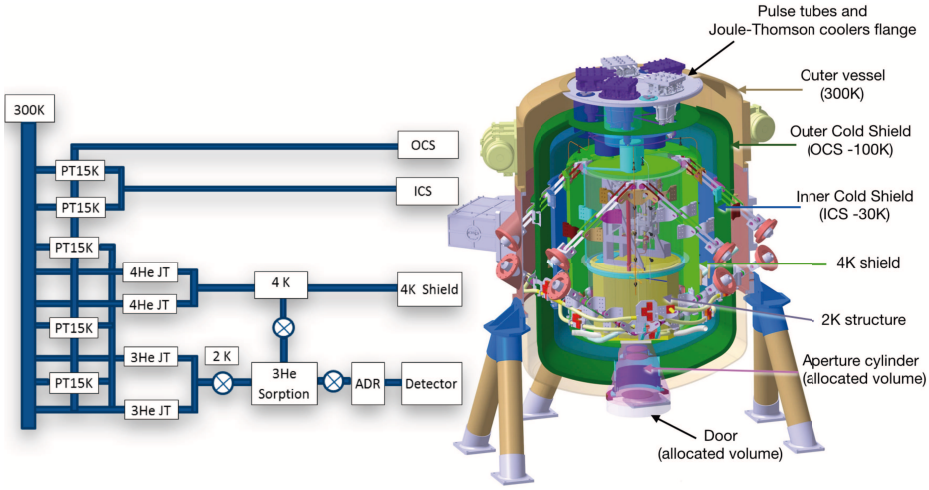

Fig. 3 X-IFU cryogenic chain baseline and dewar design (CNES)

6 Current status of the X-IFU

The current design leads to an instrument meeting the science requirements and weighing about 800 kg. The optimization of mass, electrical power and cryogenic margins is in progress. Achieving TRL 5 in key technologies is under way for the mission adoption in 2020.

Acknowledgements The X-IFU will be provided by an international consortium led by France, The Netherlands and Italy, with further ESA member state contributions from Belgium, Finland, Germany, Poland, Spain, Switzerland and two partners from outside Europe (the United States and Japan). The research leading to the results on thermal filters and non X-ray background has received funding from European Unions Horizon 2020 Program under the AHEAD project (grant agreement No. 654215). A. Rozanska was supported by Polish National Science Center grants No. 2015/17/B/ST9/03422, 2015/18/M/ST9/00541.

References

1. K. Mitsuda et al., *Proc. SPIE* **9144**, 91442A (2014) DOI:10.1117/12.2057199
2. R. Kelley et al., *Proc. SPIE* **9905**, 99050V (2016) DOI:10.1117/12.2232509
3. K. Nandra et al., *arXiv*:1306.2307 [astro-ph.HE] (2013)
4. D. Barret. et al., *Proc. SPIE* **9905**, 99052F (2016) DOI:10.1117/12.2232432
5. C. Goodwin Pappas et al., *J. Low Temp. Phys.* **This Special Issue** (2017)
6. L. Gottardi et al., *J. Low Temp. Phys.* **This Special Issue** (2017)
7. N. Wakeham et al., *J. Low Temp. Phys.* **This Special Issue** (2017)
8. K. Sakai et al., *J. Low Temp. Phys.* **This Special Issue** (2017)
9. P. Khosropanah et al., *J. Low Temp. Phys.* **This Special Issue** (2017)
10. A. Miniussi et al., *J. Low Temp. Phys.* **This Special Issue** (2017)
11. K. Nagayoshi et al., *J. Low Temp. Phys.* **This Special Issue** (2017)
12. M. Ridder et al. , *J. Low Temp. Phys.* **This Special Issue** (2017)
13. P. Peille et al., *J. Low Temp. Phys.* **This Special Issue** (2017)
14. R. den Hartog et al.,, *J. Low Temp. Phys.* **This Special Issue** (2017)
15. H. Hakamatsu et al., *J. Low Temp. Phys.* **This Special Issue** (2017)
16. M. Bruijn et al., *J. Low Temp. Phys.* **This Special Issue** (2017)
17. N. DeNigris et al., *J. Low Temp. Phys.* **This Special Issue** (2017)
18. D. Prêle et al., *J. Low Temp. Phys.* **This Special Issue** (2017)
19. J. van der Kuur et al., *J. Low Temp. Phys.* **This Special Issue** (2017)
20. E. Cucchetti et al., *J. Low Temp. Phys.* **This Special Issue** (2017)
21. C. Macculi et al., *Proc. SPIE* **9905**, 99052K (2016) DOI 10.1117/12.2231298
22. M. Biasotti et al., *J. Low Temp. Phys.* **This Special Issue** (2017)
23. M. D'Andrea et al., *J. Low Temp. Phys.* PE-52 **This Special Issue** (2017)
24. M. D'Andrea et al., *J. Low Temp. Phys.* PE-53 **This Special Issue** (2017)
25. S. Lotti et al., *Exp. Astron.* (2017) DOI 10.1007/s10686-017-9538-1
26. A. Miniussi et al., *J. Low Temp. Phys.* **176**, 815 (2014) DOI 10.1007/s10909-014-1104-x
27. S. Stever et al., *J. Low Temp. Phys.* **This Special Issue** (2017)
28. M. Barbera et al., *J. Low Temp. Phys.* **184**, 706 (2016) DOI 10.1007/s10909-016-1501-4
29. M. Barbera et al., *J. Low Temp. Phys.* **This Special Issue** (2017)
30. L. Sciortino et al., *J. Low Temp. Phys.* **This Special Issue** (2017)
31. N. Yamasaki et al., *J. Low Temp. Phys.* **This Special Issue** (2017)